DOI: 10.26599/FSHW.2025.9250819

Contents lists available at SciOpen

Food Science and Human Wellness

journal homepage: https://www.sciopen.com/journal/2097-0765

China Food Publishing Co.

Interaction between foodborne carbon dots and cadmium mediates synergistic escalation of toxicity: Bioaccumulation-driven oxidative stress aggravates colonic injury

Shihu Yang, Xu Guo, Sheng Wang, Xu Tian, Qianqian Yu, Yingjie Wang, Dai Cheng*

State Key Laboratory of Food Nutrition and Safety, Tianjin University of Science & Technology, Tianjin, 300457, China

ABSTRACT: Food-borne carbon dots (FCDs) are ubiquitous nanoparticles in food thermal processing, which might co-occur with persistent environmental pollutants and pose potential health risks. Cadmium (Cd) is a common harmful heavy metal pollutant in the environment. However, the interaction between FCDs and Cd and the biotoxic effects of the resultant complexes (FCDs-Cd) on organisms remain almost entirely unexplored. Herein, TEM, FTIR, XPS, and ITC were utilized to analyze the interaction between FCDs and Cd. Based on this, zebrafish and mice were employed as model animals to explore the exposure of FCDs-Cd. The results illustrated that FCDs spontaneously interacted with Cd to form FCDs-Cd. Furthermore, exposure to FCDs-Cd caused 2.73-fold higher mortality in zebrafish and exacerbated developmental abnormalities. Moreover, accumulation of FCDs-Cd was found in the liver, kidney, and intestine of mice, which led to redox homeostasis imbalance and reactive oxygen species overproduction. Furthermore, FCDs-Cd caused 4-fold higher Cd accumulation in the colon than the Cd group, resulting in more pronounced damage. Transcriptome analysis further revealed that the FCDs-Cd may induce colonic injury in mice via activating the Syk/Btk/NF-κB pathway. This study provides novel perspectives for assessing the health risks of endogenous nanoparticles and heavy metals.

Keywords: Foodborne carbon dots; Cadmium; Interaction; Bioaccumulation; Oxidative stress; Synergistic toxicity

1. Introduction

In recent years, nanoparticles (NPs) have gained widespread application in medicine, food, chemicals, and energy owing to their small particle size, large specific surface area, and favorable permeability [1,2]. However, the potential health risks to humans have led to the recognition of NPs as emerging environmental contaminants. Numerous studies have shown that exogenous engineered NPs could infiltrate cells and trigger oxidative stress, genotoxicity and neurotoxicity [3]. Furthermore, NPs could serve as carriers for the complexation of heavy metals in the environment due to the relatively large specific surface area and adhesion. These metal-NPs could utilize the carrier effect of NPs to infiltrate the cells that individual metals usually cannot access, thereby significantly amplifying the toxicity of metals by affecting their bioaccumulation, metabolism, and distribution within organisms [4,5]. NPs are not limited to

***Corresponding author**
dcheng@tust.edu.cn (Dai Cheng)

Received 13 May 2025
Received in revised from 10 June 2025
Accepted 10 July 2025

nanoscale-engineered materials, the potential toxicity and biological effects of endogenous NPs originating from foodstuffs have attracted attention [6].

Foodborne carbon dots (FCDs) represent a novel type of endogenous NPs generated during food processing, characterized by a size of less than 10 nm, and primarily constituted by carbon, oxygen, hydrogen, and/or nitrogen [7,8]. To date, FCDs have been extensively identified in a variety of food products, including vegetable, fruit wastes, protein by-products, and microbial [9-11], suggesting their ubiquitous presence in food processing. This implies that humans have been unknowingly exposed to these previously unrecognized nanostructures for an extended period. When FCDs are inevitably ingested, they could be absorbed into the digestive system and potentially accumulate within organisms, posing a health hazard [7]. The study by Song et al. [12] demonstrated that FCDs from grilled Atlantic salmon could induce cells apoptosis and cause changes in energy production pathways. Meanwhile, FCDs could disrupt the gut microbiota, inducing intestinal inflammation and intestinal mucus layer destruction [13]. In addition, it is worth noting that FCDs have hydroxyl, amino, and carboxyl functional groups on their surfaces [14], providing convenient conditions for interacting FCDs with exogenous compounds. Studies have shown that these functional groups could promote the interaction between FCDs and metal ions, thereby exerting effects in multiple fields. FCDs could chelate Zn and Fe, serving as micronutrient supplements [15,16]. Furthermore, FCDs could form ground-state complexes with Mn and Cr that could be used as fluorescent sensors for the detection of hazardous substances [17].

Cadmium (Cd) is a common heavy metal pollutant with significant hazard and persistent risk, which can induce harmful effects even at low concentrations. Cd is capable of entering the body via the food chain and accumulates in the kidney, liver, and gut [18,19]. This may lead to altered nutrient digestibility [20], disruption of the gut microbiota [21], and inflammatory response, thereby increasing disease susceptibility. Cd has been identified as a key food contaminant, the International Agency for Research on Cancer (IARC) has classified it as the Group I human carcinogen [22]. Moreover, the combined toxicity of Cd and NPs has attracted much attention. As elucidated by Teng et al. [5], the administration of ZnO NPs and Cd instigated endothelial cell shedding and lowered levels of tight junction proteins, exacerbating the damage to the placental barrier. Similarly, the combined exposure of SiNPs and Cd induced liver damage and increased the accumulation of Cd [23]. These findings suggested that the combined effects of NPs and Cd could cause negative health consequences. Based on this, it is reasonable to suspect that Cd may achieve efficient transmembrane transport through the carrier effect of FCDs, leading to higher Cd accumulation in the organism. However, the interaction mechanism between FCDs and Cd as well as the deleterious effects of FCDs-Cd complexes have not been explored.

In this study, we prepared FCDs-Cd complexes and investigated the structural characteristics and interaction mechanism of FCDs-Cd by characterizing their particle size, elemental composition, optical properties, surface chemical groups, and thermodynamic parameters. Additionally, zebrafish and mice were chosen as the experimental models for the assessment of the toxicity of FCDs-Cd by measuring

biodistribution, biochemical indicators, and transcriptome-level responses. This work was intended to shed light on the potential health risks associated with the complexes produced by the interaction of FCDs and Cd.

2. Materials and Methods

2.1 Chemicals

Cadmium chloride ($CdCl_2$) was sourced from Damao Chemical Reagent Factory (Tianjin, China). All other chemicals were acquired from different local suppliers. Unless otherwise indicated, all chemicals were of analytical reagent grade. Besides, all required assay kits were procured from Nanjing Jiancheng Bioengineering Institute.

2.2 Preparation of FCDs-Cd

Fresh pork (300 g) was cut into 1 cm^3 cubes and roasted at 230 ℃ for 45 min. Anhydrous ethanol was incorporated in a ratio of 1:10, stirred for 12 h, and sonicated for 15 min. After removing large insoluble particles, the ethanol was evaporated, and then the mixture was subsequently solubilized by adding deionized water. The samples obtained by extraction with dichloromethane were filtered by 0.22 μm membrane and then placed in the dialysis bag (500 Da) for 24 h, with the solution being changed every 4 h. The inner dialysate was collected, lyophilized under vacuum, and the resulting powder was stored at low temperature [24]. Then, the FCDs and Cd were mixed evenly according to the mass ratio of 4:1 and thereafter placed in a 50 ℃ water bath for 30 min. The mixture was transferred into the dialysis bag (500 Da) for 24 h, changing the solution every 4 h to eliminate free Cd ions. Subsequently, the dialysate was collected and freeze-dried [15].

2.3 Characterization of FCDs-Cd

Transmission electron microscopy (TEM, Talos F200X G2, USA) was employed to analyze the shape and size of FCDs and FCDs-Cd. A full-wavelength ultraviolet-visible spectrophotometer was used to determine the ultraviolet-visible spectra of FCDs and FCDs-Cd in the range of 200-600 nm (Lambda 35, PerkinElmer, USA). The fluorescence was assessed utilizing a fluorescence spectrometer (RF6000, Shimadzu, Japan). The elemental composition of FCDs and FCDs-Cd was determined by X-ray photoelectron spectroscopy (XPS, ESCALAB250, USA). The surface groups of FCDs and FCDs-Cd were acquired by Fourier-transform infrared spectroscopy (FT-IR, Nicolet iS50, USA).

2.4 Isothermal Titration Calorimetry

The interaction thermodynamics of FCDs with Cd were examined by Isothermal titration calorimetry (ITC, ITC-200, USA). FCDs and Cd were dissolved in PBS and filtered via microporous membrane (0.22 μm) to eliminate larger particles. Following degasification, 2 mmol/L Cd was titrated into 5 mmol/L FCDs, with the Cd solution titrated into deionized water as the control. The collected data was analyzed using the Nano Analyze software and determined the association constant (Ka), enthalpy (ΔH), entropy (ΔS), and Gibbs free energy (ΔG).

2.5 Animals and Treatment

Zebrafish were provided by the Tianjin International Joint Academy of Biomedicine (Tianjin, China) and reared in a recirculating culture system at a water temperature of 25 ± 1 ℃ for 14 h light and 10 h dark cycles. Females and males aged 6-12 months were housed at a 2:1 ratio in filtered tap water with dissolved oxygen > 80% and pH 7.4 ± 0.5. Zebrafish were fed with shrimp twice a day, and half of the aerated water was changed every two days. Two male adult zebrafish and one female adult zebrafish were placed in a breeding box for natural spawning. The zebrafish eggs were cultured in the medium for 6 h, and then randomly divided into control, low-dose $CdCl_2$ (LCd, 8 mg/L), high-dose $CdCl_2$ (HCd, 16 mg/L), low-dose FCDs-$CdCl_2$ (LFCDs-Cd, 8 mg/L), high-dose FCDs-$CdCl_2$ (HFCDs-Cd, 16 mg/L), and FCDs (132 mg/L), with a minimum of 20 larvae per treatment group. The concentration of Cd was selected referring to the earlier research [25].

Six-week-old male C57BL/6 mice were acquired from Sibeifu (Beijing) Biotechnology Co., Ltd. All animal experiments followed the Ethics Committees for Animal Research of Tianjin University of Science and Technology (Approval No. 2024068). The mice were kept in an environment with a humidity of 60% and a temperature of 25 ± 2 ℃, under a 12 h dark/light photoperiod, the food and water were accessed ad libitum. Following one week of acclimatization, the mice were haphazardly sorted into six groups (10 mice in each group), namely control, low-dose $CdCl_2$ (LCd, 12.5 mg/kg), high-dose $CdCl_2$ (HCd, 25 mg/kg), low-dose FCDs-$CdCl_2$ (LFCDs-Cd, 12.5 mg/kg), high-dose FCDs-$CdCl_2$ (HFCDs-Cd, 25 mg/kg), and FCDs (206 mg/kg). The Cd concentration was based on previous research [26]. The control group mice were orally administered a 0.9% NaCl solution. The mice in the FCDs group and HFCDs-Cd group were executed by cervical dislocation at 3, 6 and 24 h after administration. The fluorescence distribution of organs was observed using a small animal live imager (Tanon ABL X5, China). For acute oral toxicity studies, the remaining mice were sacrificed by cervical dislocation 24 h post-exposure. The blood and tissue samples were collected from the mice and stored at -80 ℃ for future use.

2.6 Determination of Biochemical Indicators

The levels of urea nitrogen (BUN, C013-2-1) and creatinine (Cr, C011-2-1), aspartate aminotransferase (AST, C010-2-1), alanine aminotransferase (ALT, C009-2-1) in serum, and superoxide dismutase (SOD, A001-1), malondialdehyde (MDA, A003-2), reduced glutathione (GSH, A006-2-1), myeloperoxidase (MPO, A044-1-1) and nitric oxide (NO, A013-2-1) in tissues were all determined by the kits. The protein concentration was measured by BCA protein assay (BCA kit, PC0020).

2.7 Histological Analysis

The colon was immersed in 4% paraformaldehyde, and paraffin sections were obtained by soaking, embedding, and slicing. Paraffin sections were stained with hematoxylin and eosin (H&E) for histopathological observation. The goblet cells density and mucus layer thickness in colon were monitored by the Alcian blue-periodic acid Schiff (AB/PAS).

2.8 Determination of Cd Content

The sample (about 0.1 g) was digested in a nitrification tube with 5 mL HNO_3 and 2 mL H_2O_2, and then finalized with deionized water to 50 m L. Using the 1% nitric acid solution as a blank, 10 mL of the solution was taken for determination by plasma mass spectrometry (ICP-MS, ICAPQ, Thermo Fisher) [27].

2.9 Transcriptome Sequencing and Validation

Total RNA was isolated from mouse colon tissue by means of Trizol reagent. The concentration, purity, and integrity of RNA were evaluated by NanoDrop 2000 spectrophotometer and Agilent 2100/LabChip GX system. After confirming the sample quality, double-stranded cDNA was synthesized step by step. A high-quality cDNA library was constructed by purification, repair, A-tailing, adapter ligation, and fragment size selection. The library was subsequently enriched by PCR amplification quality assurance. The qualified libraries underwent high-throughput sequencing in PE150 mode on the Illumina NovaSeq6000 platform. The raw data was strictly filtered and aligned to the reference genome. According to the comparison results, the expression of each gene was computed, and the samples were subjected to differential expression and enrichment analysis. The cDNA of the sample was subjected to RT-PCR using the SYBR Green kit (Tiangen, China) in a Bio-Rad CFX Connect system (Bio-Rad, USA). Primer sequences were designed by Primer-BLAST of NCBI (Table S1). GAPDH was employed to normalize the mRNA relative expression.

2.10 Statistical Analysis

All experiments were performed with at least three independent replications. Data were presented as mean ± standard error (SEM) and plotted by GraphPad Prism 8. The normality of the data was assessed using the Shapiro-Wilk test in SPSS 26.0. Data conforming to the normal distribution were analyzed using one-way analysis of variance (ANOVA), with Levene's test used to evaluate the homogeneity of variances. Significant differences were determined using the Student-Newman-Keuls (SNK) multiple comparisons test [28], with $P < 0.05$ indicating statistical significance.

3. Results

3.1 Characterization of FCDs-Cd

The TEM was used to observe the morphology of FCDs and FCDs-Cd (Figs. 1A and B), and it could be seen that the FCDs presented nearly spherical NPs in a uniform distribution without significant aggregation. The average particle sizes of FCDs and FCDs-Cd were 2.04 nm and 2.25 nm, respectively (Figs. 1A and B, inset). The UV-vis absorption spectra displayed a distinct absorption peak ascribed to π-π* electronic transition in C=C at 240 nm (Fig. 1C), suggesting that FCDs exhibit a unique fluorescence emission capability. Besides, the FCDs and FCDs-Cd exhibited blue fluorescence under UV irradiation. The fluorescence spectra of FCDs and FCDs-Cd were presented at different excitation wavelengths (Figs. 1D and E). The maximum excitation wavelengths of FCDs and FCDs-Cd were 380 nm and 370 nm, respectively. Meantime, the maximum excitation wavelength and the fluorescence intensity of FCDs decreased upon binding with Cd, suggesting that Cd may cause fluorescence quenching on FCDs. Furthermore, the maximum emission wavelength was red-shifted with increasing excitation wavelength.

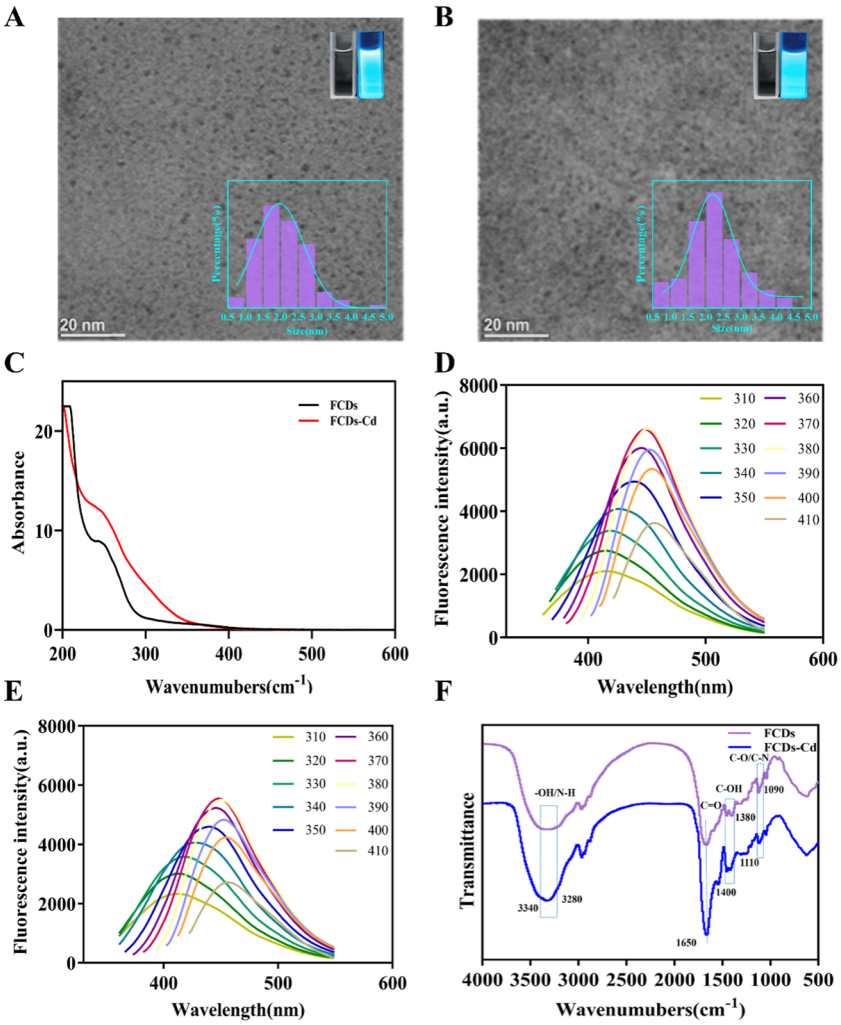

Fig. 1 TEM images of (A) FCDs and (B) FCDs-Cd. The insets show the size distribution and photographs under UV light of FCDs and FCDs-Cd. UV-vis absorption spectra of (C) FCDs and FCDs-Cd. Fluorescence emission spectra of (D) FCDs and (E) FCDs-Cd. FTIR spectra of (F) FCDs and FCDs-Cd.

Subsequently, FTIR was employed to analyze the surface functional groups (Fig. 1F). The broad peak of FCDs at 3340 cm^{-1} was recognized as the stretching vibrations of O-H and N-H, and the spectral band near 1650 cm^{-1} was associated with the C=O stretching vibration. The peak at 1380 cm^{-1} represented the deformation peak of C-OH, and the 1110 cm^{-1} peak was attributed to C-O and C-N stretching vibrations. Upon binding with Cd, the peak intensities at 3340, 3280, and 1650 cm^{-1} were augmented, and the C-OH at 1380 cm^{-1} moved to 1400 cm^{-1}, while the C-O/C-N at 1090 cm^{-1} shifted to 1110 cm^{-1}, which confirmed that the amino, hydroxyl, and carboxyl groups on the surface of FCDs were involved in bound to Cd. Additionally, the EDS elemental mapping results indicated that FCDs consisted of the elements C, N, and O (Fig. S1A), while the FCDs-Cd composed of C, N, O, and Cd (Fig. S1B).

The high-resolution XPS spectroscopy further confirmed the functional groups on FCDs. The results displayed three main peaks at 285, 400, and 532 eV attributed to the elements C, N, and O (Fig. 2A), respectively, which was in accordance with the result obtained from EDS mapping. The high-resolution C1s peaks validated the absence of C=C, C-O/C-N, and C=O bonds with peaks at 284.9, 286.1, and 288.2 eV, respectively (Fig. 2B). The high-resolution N1s spectrum showed characteristic peaks for pyridinic N, amine N, and protonated amine at 398.9, 399.8, and 400.5 eV, respectively (Fig. 2C). The high-resolution O1s

spectrum exhibited peaks corresponding to C=O, O=C-O, and C-O at 530.9, 531.8, and 532.9 eV, respectively (Fig. 2D). In addition, it could be seen from the XPS spectra of FCDs-Cd that the binding energies of the high-resolution spectra of C1s, N1s, and O1s were altered compared with those of FCD (Figs. 2E-H), indicating the engagement of amino, hydroxyl, and carboxyl groups in the interaction between FCDs and Cd. Further analysis of the high-resolution Cd3d spectra showed two characteristic peaks near 405.2 and 411.8 eV (Fig. 2I), suggesting that Cd was bound to the surface of FCDs. The schematic diagram in Fig. 2J further explains the formation of FCDs-Cd.

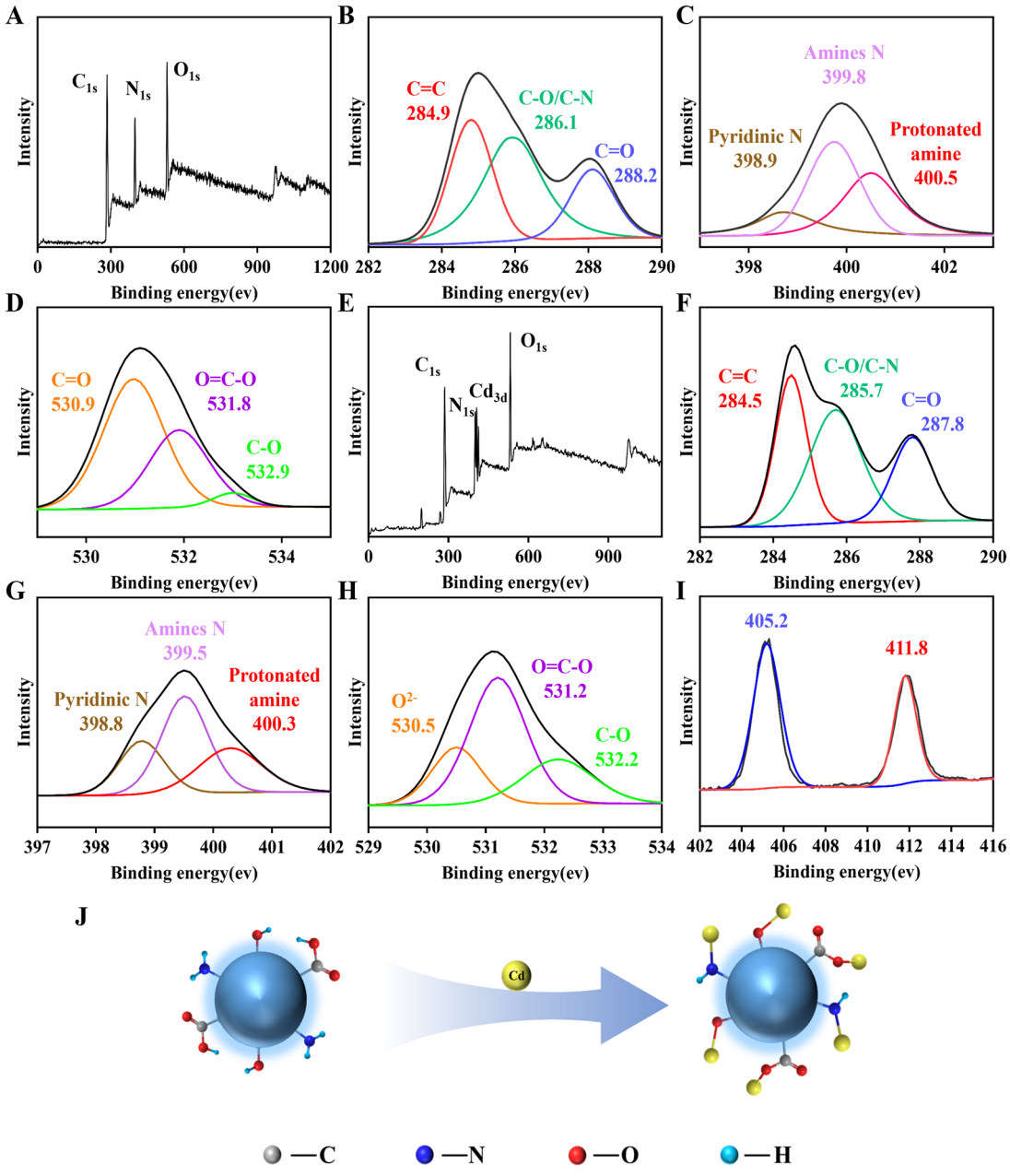

Fig. 2 (A) XPS spectrum and high-resolution (B) C1s, (C) N1s and (D) O1s spectra of FCDs. (E) XPS spectrum and high-resolution (F) C1s, (G) N1s, (H) O1s and (I) Cd3d spectra of FCDs-Cd. (J) Synthesis diagram of the FCDs-Cd complexes.

3.2 Thermodynamic Analysis

ITC was used to inspect the interaction of FCDs with Cd, and the thermodynamic parameters including ΔH, ΔG, and ΔS were obtained from the binding curve, which could be used to calculate the molecular

interaction by calorimetric techniques [29]. As depicted in Fig. S2, the dilution plot was downward, indicating an exothermic process. After correcting the change of dilution heat, the titration curve was fitted using nonlinear least squares. At 298 K, the Ka was 1.45×10^3 M^{-1}. The interaction between FCDs and Cd resulted in $\Delta H = -2.70 \pm 0.48 \times10^4$ J/mol, $\Delta S = -29.9$ J/mol/K, and $\Delta G < 0$. Thermodynamic parameters indicated that the entropy change contributed less to the free energy of the reaction, the reaction between FCDs and Cd was mainly driven by enthalpy change.

3.3 Effects of FCDs-Cd on Development in Zebrafish

Zebrafish, a well-established model organism, has been broadly applied to study ecotoxicology for its short life cycle, rapid development and growth [30]. The stereomicroscope was first utilized to observe the morphological changes in zebrafish embryos. After 24 hours post fertilization (hpf), the embryos in the HCd group showed reduced melanocytes and slow development, whereas the HFCDs-Cd group displayed the interruption of embryonic development and more pronounced damage (Fig. 3A). Furthermore, it was found that the hatching rate in the HFCDs-Cd group was 0.61 times that of the HCd group (Fig. 3B). The mortality of zebrafish within 4 days post fertilization (dpf) after administration was shown in Fig. 3C. Compared with the control, a dose-dependent elevation in mortality was noticed in both the Cd and FCDs-Cd groups of zebrafish. Under the same Cd concentration, the mortality rate of HFCDs-Cd group was 2.73 times higher than HCd group. Meanwhile, in contrast to the control group at 4 dpf, zebrafish in the LCd group presented spinal curvature, the LFCDs-Cd group manifested yolk sac edema and melanocyte reduction, while the HFCDs-Cd group endured severe tail deformation, circulation defects and pericardial edema (Fig. 3D). The body length was reduced by 11.93% in the HFCDs-Cd group with respect to the HCd group (Fig. 3E). Moreover, the Cd level of HFCDs-Cd group was pronouncedly higher than other groups (Fig. 3F). Consistently, the changes of MDA content and SOD activity in FCDs-Cd group further confirmed the above results (Figs. 3G and H). These results demonstrated that exposure to FCDs-Cd aggravated their toxic effects on zebrafish.

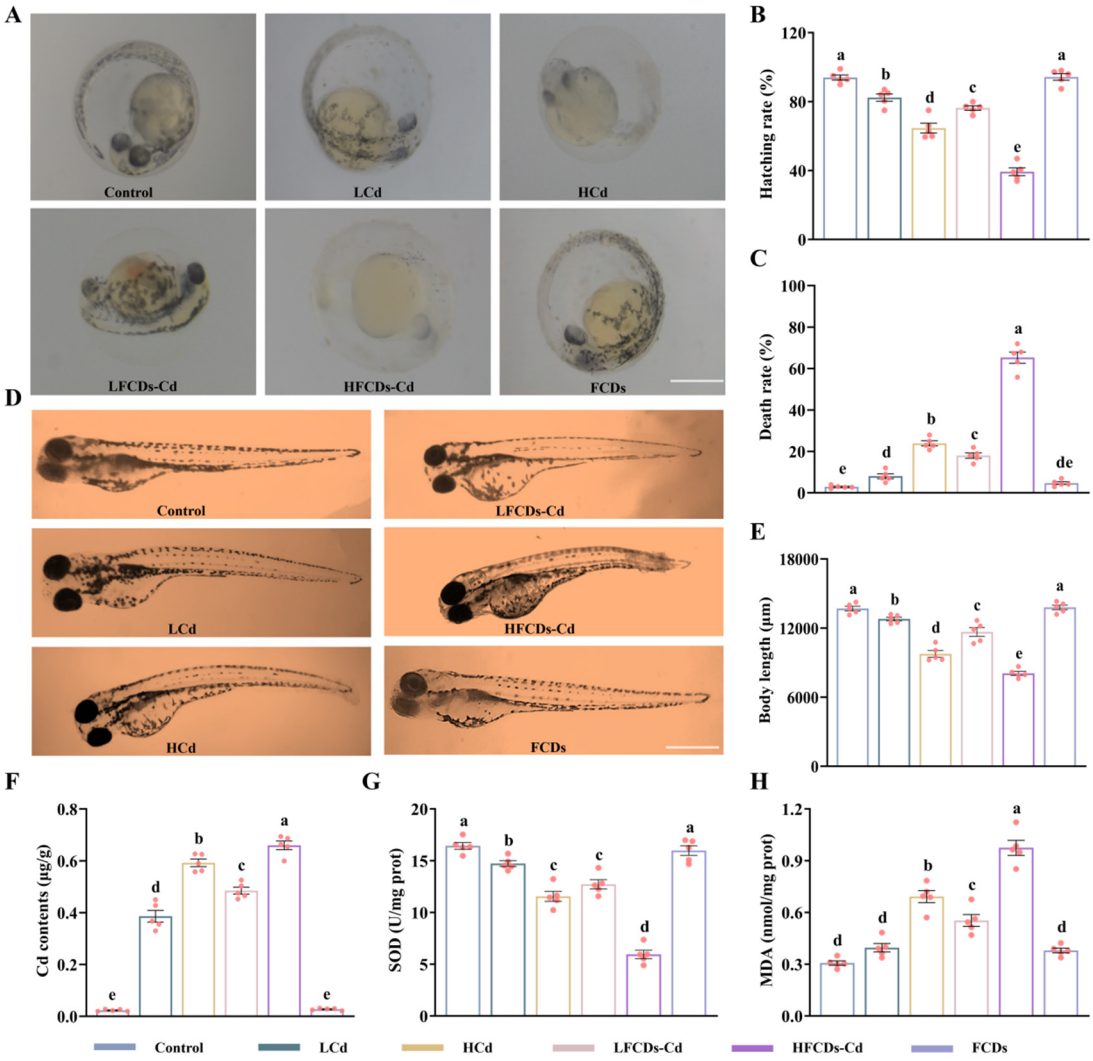

Fig. 3 FCDs-Cd induced growth and developmental retardation in zebrafish. (A) Embryonic development at 24 hpf (scale =500 μm). (B) Hatching rate at 4 dpf. (C) Death rate at 4 dpf. (D) Phenotype changes at 4 dpf (scale =3000 μm). (E) Body length at 4 dpf. (F) Cd contents. (G) SOD content. (H) MDA content. Data were expressed as mean ± SEM (n=5) with different lowercase letters representing statistical significance ($P < 0.05$).

3.4 Biodistribution of FCDs-Cd in Mice

Based on the fluorescence characteristics of FCDs, a small animal live imager was used to observe the biodistribution of FCDs and HFCDs-Cd in the major organs of mice at 3, 6, and 24 h post-oral gavage. As shown in Fig. 4, the enhanced fluorescence signals were found in the stomach, intestine, liver, spleen, kidney, and brain, 3 h after administration of the drugs. The fluorescence intensity of each tissue gradually decreased 6 h after administration and approached the initial level at 24 h. This indicated that HFCDs-Cd and FCDs may be absorbed and subsequently excreted in the urine and/or feces. Subsequently, we carried out further determination of Cd content to explore the impact of FCDs on Cd uptake and translocation. In contrast to the HCd group, the Cd contents in the liver, kidney, spleen, and colon of the HFCDs-Cd group increased by 1.67, 2.05, 1.76, and 1.37 times, respectively, but there was no significant difference in the brain. In particular, the Cd content in the LFCDs-Cd group was over 4 times that in the LCd group in the colon (Table 1), indicating that FCDs promoted Cd uptake.

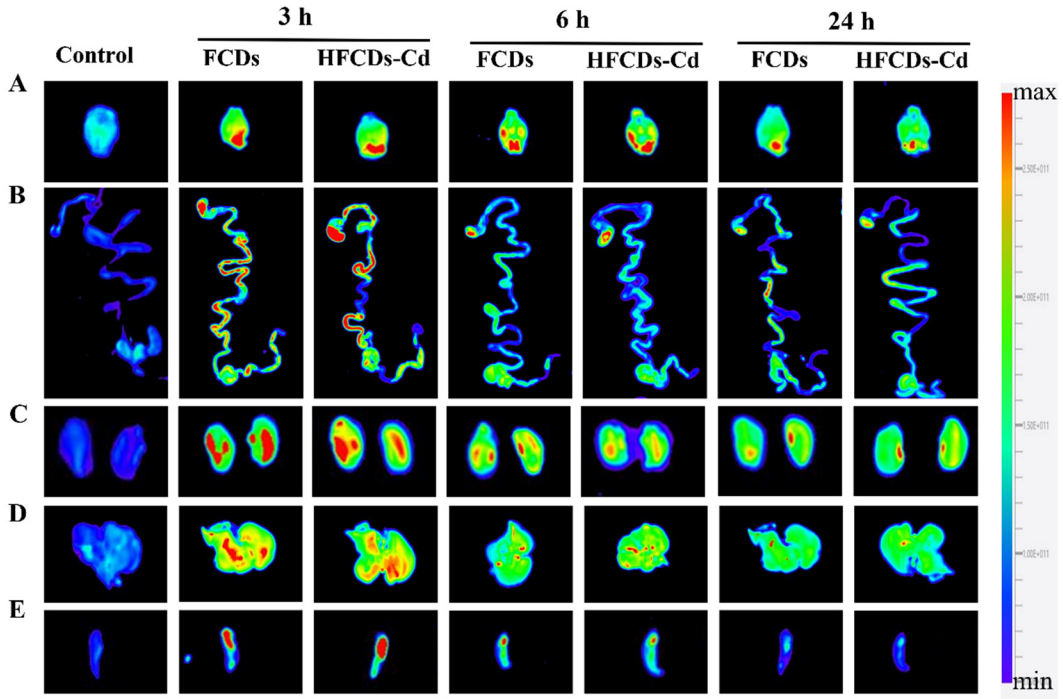

Fig. 4 Ex vivo fluorescence images of (A) brain, (B) stomach and intestine, (C) kidney, (D) liver, and (E) spleen of mice orally administrated with FCDs and HFCDs-Cd at 3, 6, and 24 h, respectively.

Table 1 Cd contents in mouse tissues (μg/g)

Group	Control	LCd	HCd	LFCDs-Cd	HFCDs-Cd	FCDs
Brain	0.002 ± 0.001^{c}	0.005 ± 0.001^{b}	0.011 ± 0.001^{a}	0.007 ± 0.001^{b}	0.012 ± 0.001^{a}	0.002 ± 0.001^{c}
Liver	0.089 ± 0.009^{e}	0.657 ± 0.059^{d}	9.567 ± 0.932^{b}	2.339 ± 0.331^{c}	16.016 ± 2.040^{a}	0.090 ± 0.003^{e}
Kidney	0.108 ± 0.019^{d}	0.492 ± 0.063^{c}	0.939 ± 0.085^{b}	0.828 ± 0.091^{b}	1.927 ± 0.299^{a}	0.092 ± 0.007^{d}
Spleen	0.002 ± 0.001^{e}	0.141 ± 0.023^{d}	0.523 ± 0.077^{b}	0.342 ± 0.071^{c}	0.920 ± 0.103^{a}	0.002 ± 0.001^{e}
Colon	0.021 ± 0.004^{e}	0.993 ± 0.109^{d}	5.293 ± 0.627^{b}	4.008 ± 0.499^{c}	7.266 ± 1.002^{a}	0.015 ± 0.006^{e}
Feces	0.036 ± 0.005^{c}	15.317 ± 1.829^{b}	62.631 ± 4.621^{a}	14.362 ± 1.709^{b}	64.217 ± 4.932^{a}	0.031 ± 0.009^{c}

Note: Different letters indicate significant differences ($P < 0.05$).

3.5 Effects of FCDs-Cd on Liver and Renal Function in Mice

The liver acts as an important metabolic organ of the body. We explored the effects of complex exposure to FCDs and Cd on liver function and oxidative stress in mice. As presented in Figs. 5A and B, the AST and ALT in the HFCDs-Cd group were 17.61% and 22.11% higher than those in the HCd group, respectively. In addition, MDA, SOD, and GSH levels were measured to assess the effects of complex exposure to FCDs-Cd on hepatic oxidative stress. Compared with the HCd group, the MDA content in the liver was significantly increased, the GSH content and SOD activity were markedly decreased after HFCDs-Cd exposure (Figs. 5C-E).

In order to evaluate kidney function, BUN and Cr levels were quantified. Contrasted with the control group, the BUN and Cr levels were raised in complex exposure groups (LFCDs-Cd, HFCDs-Cd). The BUN and Cr contents in the HFCDs-Cd group exceeded those in the HCd group by 1.24 and 1.17 times, respectively (Figs. 5F and G). This indicated that complex exposure led to a reduction in glomerular filtration rate, which caused a significant elevation of BUN and Cr in the serum, demonstrating enhanced nephrotoxicity. Further oxidative stress analysis revealed that exposure to HCd and HFCDs-Cd decreased SOD and GSH levels, and

increased MDA levels in the kidney to varying degrees, suggesting an increase in oxidative stress (Figs. 5H-J). Moreover, the changes of oxidative stress in serum also showed the same pattern (Fig. S3A-C). Collectively, these findings suggested that FCDs-Cd treatment resulted in exacerbated liver and kidney injury.

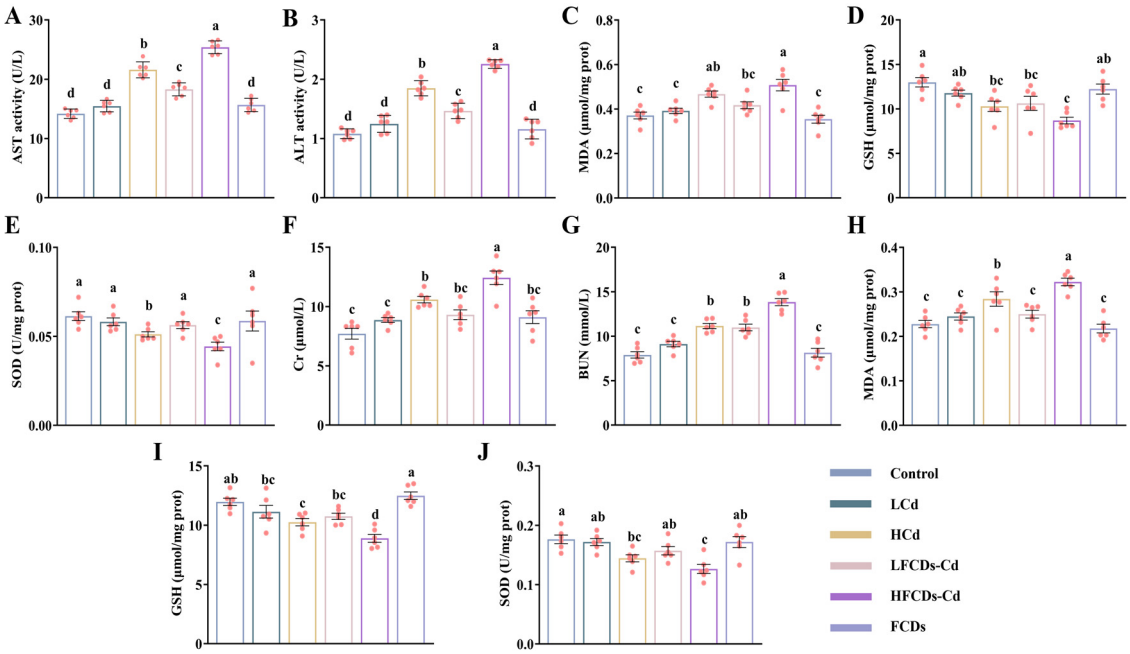

Fig. 5 FCDs-Cd induced more severe hepatic and renal injury in mice. The activities of (A) AST and (B) ALT in serum. The contents of (C) MDA, (D) GSH, and (E) SOD in the liver. The contents of (F) Cr and (G) BUN in serum. The contents of (H) MDA, (I) GSH, and (J) SOD in the kidney. Data were expressed as mean ± SEM (n=6) with different lowercase letters representing statistical significance ($P < 0.05$).

3.6 Effects of FCDs-Cd on Colon Damage in Mice

Histological examination of H&E-stained revealed that single exposure to HCd caused slight damage to the intestinal morphology and destruction of the epithelial structure, while the HFCDs-Cd induced disordered arrangement of colonic epithelial cells and shedding of cellular debris in the intestinal lumen (Fig. 6A). Furthermore, compared with the control group, exposure to HCd and HFCDs-Cd groups caused colonic crypt alteration, mucus reduction, and disordered lamina propria architecture. More significantly, the HFCDs-Cd group had more severe colonic damage (Fig. 6B). Those results implied that complex exposure caused more severe intestinal barrier damage and increased intestinal permeability than single exposure in mice, which may lead to more Cd accumulation in tissues. Further oxidative stress analysis revealed that compared with HCd group, MDA in the HFCDs-Cd group increased by 15.14%, and GSH and SOD decreased by 14.10% and 14.59%, respectively (Figs. 6C-E). Subsequently, the colon injury was evaluated by measuring the levels of NO and MPO, with the results shown in (Figs. 6F and G). Compared with the control group, the NO and MPO levels in the colon of HCd-treated mice were increased by 54.6% and 50.16%, respectively. In addition, the NO and MPO levels in the HFCDs-Cd group exceeded those in the HCd group by 1.20 and 1.12 times, respectively. Overall, these data indicated that FCDs and Cd complex exposure caused severe oxidative damage to mice compared with single treatment, demonstrating a synergistic effect.

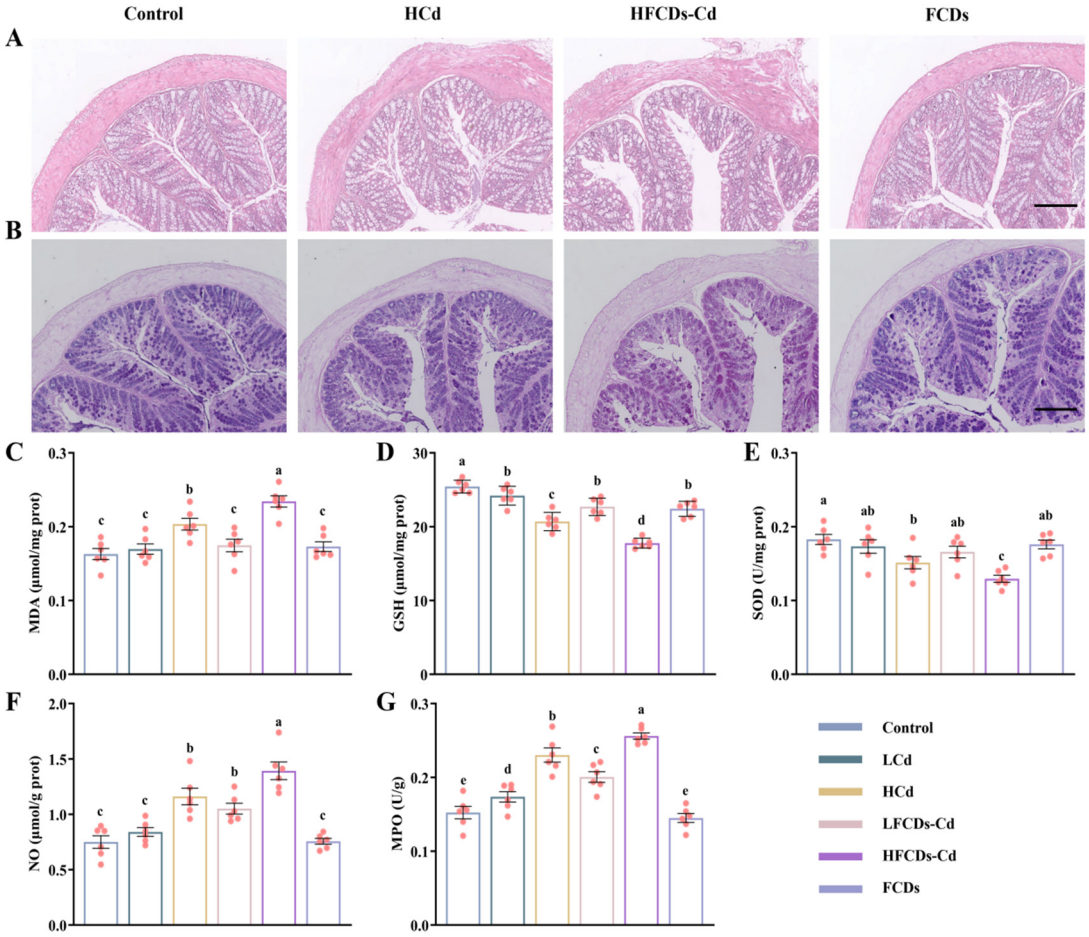

Fig. 6 FCDs-Cd induced more severe colonic injury and oxidative stress in mice. (A) H&E and (B) AB/PAS staining of colon sections (scale =250 μm). The contents of (C) MDA, (D) GSH, (E) SOD, (F) NO, and (G) MPO in the colon. Data were expressed as mean ± SEM (n=6) with different lowercase letters representing statistical significance ($P < 0.05$).

3.7 Transcriptomic Analysis

RNA-seq analysis was completed for 9 samples, yielding a total of 59.69 Gb Clean Data (5.97 Gb per sample) with a percentage of Q30 bases > 94.77%. Compared to the reference genome, the comparison efficiency of Clean Data per sample ranged from 96.36% to 97.16% (Table S2). Differentially expressed genes (DEGs) between the control and other treatments were investigated according to Fold Change≥2 and FDR<0.01. The DEGs generated by different experimental treatments were illustrated in Fig. 7A. Relative to the control, the colon of mice exposed to HCd presented 597 DEGs (459 up-regulated and 138 down-regulated), while the HFCDs-Cd exposed group had 1300 DEGs (921 up-regulated and 379 down-regulated). Thus, these findings indicated that gene transcription in the colon of mice was affected by HCd exposure and significantly disturbed by HFCDs-Cd exposure. The volcano plots depicted the up-regulation/down-regulation of DEGs in different treatments. All treatments resulted in more upregulation and less downregulation of DEGs (Figs. 7B and C). To explore the potential biological functions induced by complex exposure to FCDs and Cd, the obtained DEGs were analyzed by Gene Ontology (GO) and Kyoto Encyclopedia of Genes and Genomes (KEGG) enrichment. Gene sets from different comparative groups were categorized according to their molecular function (MF), cellular component (CC), and biological process (BP) annotations. GO functional enrichment analysis showed that DEGs in HCd vs control and HFCDs-Cd vs

control were mainly co-enriched in cellular process, biological regulation, response to stimulus, response to stimulus, and metabolic process (Figs. 7D and E). The KEGG database marked the differentially expressed gene enrichment pathways. The DEGs of HCd vs control and HFCDs-Cd vs control were enriched to 283 and 311 pathways, respectively. Among the top 20 pathways, the inflammation-related pathways B cell receptor signaling pathway, Natural killer cell mediated cytotoxicity, and NF-kappa B signaling pathway were enriched in both comparisons (Figs. 7F and G). Further analysis identified Syk, PLCy2, Btk, Prkcb, Nfatc1, and Ptpn6 as key differentially expressed genes. To verify the precision of the transcriptome sequencing results, we selected 6 DEGs for qPCR validation, and the results were in agreement with the transcriptome sequencing (Fig. S4), which affirmed the accuracy of the RNA-seq results.

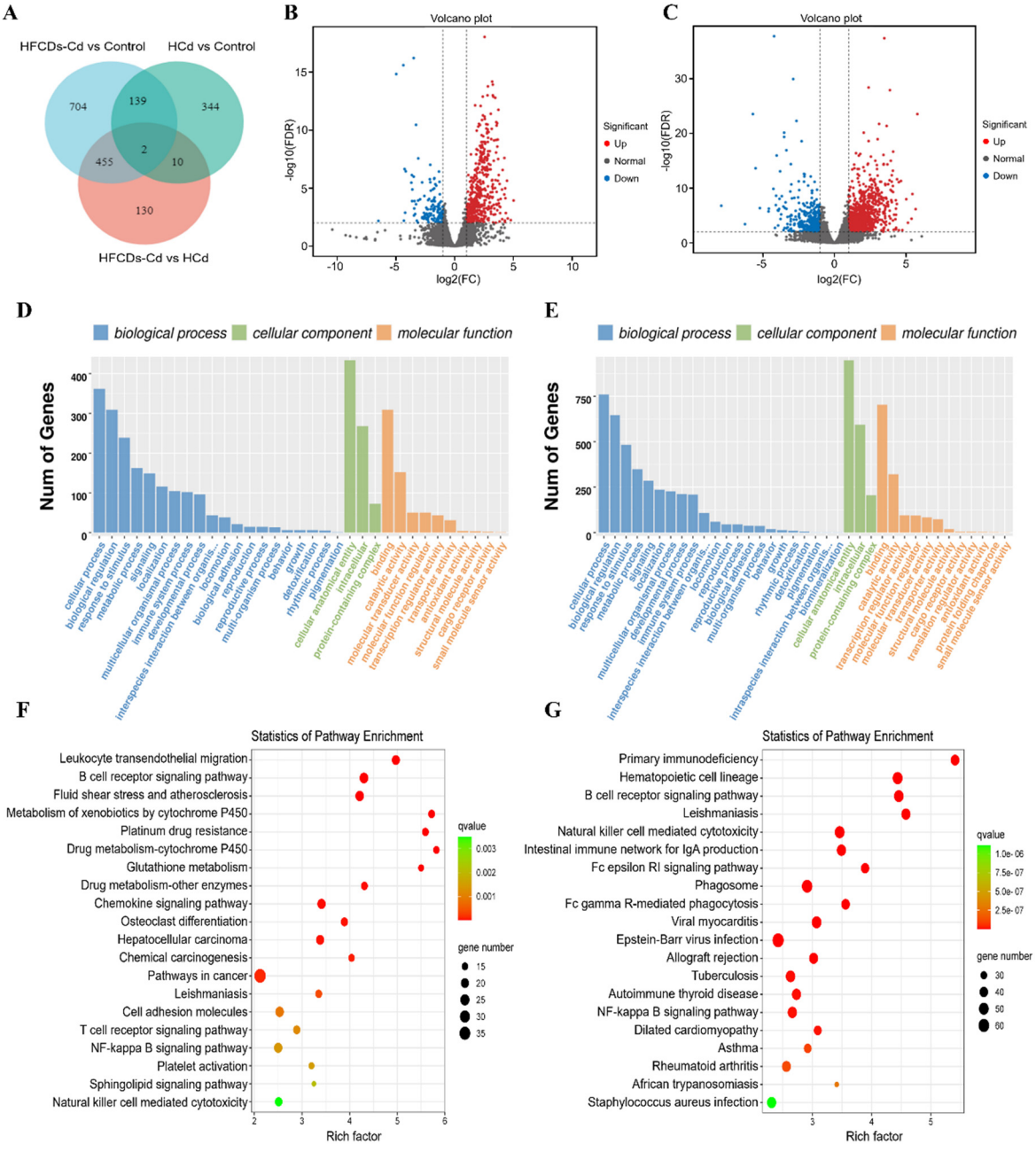

Fig. 7 Transcriptomic analysis. (A) The Venn and volcano plots of DEGs in colon exposed to (B) HCd and (C) HFCDs-Cd compared with the Control group. Enrichment analysis of GO term based on the DEGs in (D) HCd vs Control and (E) HFCDs-Cd vs Control. The histogram of the KEGG pathways of DEGs in (F) HCd vs Control and (G) HFCDs-Cd vs Control.

4. Discussion

Currently, the coexistence of NPs and heavy metals cannot be overlooked. Studies have shown that NPs could effectively adsorb heavy metals and other contaminants from the environment own to their remarkably high specific surface area properties [31]. The accumulation of FCDs and Cd in organisms shares similar characteristics. When these pollutants combine to form new complexes, they may produce synergistic effects during their transmission via the food chain, thereby further exacerbating unfavorable impacts on the ecological environment and human health [32]. Current investigations have shown that exposure to FCDs or Cd alone could induce oxidative stress and promote inflammatory responses, thereby leading to cell damage [33-35]. However, research on biological health impacts of complex exposure to FCDs and Cd remains insufficient.

In this study, we found that the particle size did not change significantly after the binding of FCDs to Cd. In the UV-vis spectra of FCDs-Cd, a new absorption peak around 246 nm not only indicated that the structures of chromophore groups (-C=O and -COOH) and chromophore groups (-OH and -NH_2) may have changed after FCDs bound with Cd but also suggested the formation of FCDs-Cd [15]. In terms of fluorescence properties, the emission peak of FCDs-Cd exhibited a red shift as the wavelength increased, which may be attributed to distinct surface emission traps caused by the diverse functional groups on FCDs [36]. Additionally, the decrease in the fluorescence intensity of FCDs-Cd may be due to the chelating effect of Cd with FCDs, leading to changes in the surface structure of FCDs and thus reducing the fluorescence efficiency [37]. The shift in the FTIR peaks revealed the binding sites of metal ions with organic ligands in FCDs. Under Cd coordination, the band moved from 3280 cm^{-1} to 3340 cm^{-1}, which was due to the formation of coordination bonds between nitrogen atoms and Cd, with Cd-N bonds replacing N-H hydrogen bonds. Meanwhile, the chelation of FCDs with Cd resulted in a significant enhancement of the spectral bands of the corresponding carboxyl groups, suggesting that the carboxyl groups were involved in the interaction of FCDs with Cd. From the XPS spectra of FCDs-Cd, the presence of atoms of C, O, N, and Cd was strong evidence for the formation of the FCDs-Cd. The Cd3d peak was deconvoluted into two peaks located at 405.2 and 411.8 eV, suggesting that the carboxyl and hydroxyl groups in FCDs combined with Cd to form Cd-O functional groups [5,38]. These results collectively indicated that Cd may interact with the oxygen of carboxyl or hydroxyl groups as well as the nitrogen of amino groups in FCDs, similar to other metal-bound FCDs [29]. Additionally, the Ka was relatively moderate compared to other interactions (K values of 10^3-10^6) [15,24], which indicated stable interaction between FCDs and Cd.

In vivo fluorescence distribution demonstrated that the fluorescence intensity was the strongest at 3 h and gradually decreased after 24 h. Consistently, the research by Wang et al. [39] showed that beer FCDs were eliminated from the mice within 24 h after ingestion. Interestingly, the FCDs-Cd exhibited a similar distribution trend to FCDs, suggesting that the amalgamation of FCDs with Cd did not alter the distribution of FCDs *in vivo*. This might provide convenient conditions for altering the absorption and distribution of Cd *in vivo*. In general, Cd absorption rates in organisms are generally low, only 0.5%-8% in rodents [40]. *In vivo*

analysis of Cd distribution revealed a considerable rise in Cd levels inside tissues and organs following treatment with FCDs-Cd, which suggested that liver, kidney, spleen and colon are the targets of Cd. This was analogous to the findings of Chen et al. [41], who demonstrated that co-exposure to microplastics and Cd led to a 1.17-1.38-fold augmentation in Cd accumulation in mice tissues. Notably, the intestine barrier is the first line of defense against harmful substances entering the human circulation. FCDs-Cd exposure may compromise the integrity of the intestinal barrier and enhance mucosal permeability. After absorption by the gastrointestinal tract, FCDs-Cd could then enter the gastrointestinal tract and blood circulation system, reaching organs such as the liver, kidney, and spleen via metal transporters [42,43], which may provoke systemic inflammatory response. As the main metabolic organ, the liver has a strong ability to metabolize and detoxify FCDs-Cd, and is vulnerable to oxidative stress damage. The kidney is susceptible to the toxicity of heavy metals due to its filtration function. It was evident that the distribution of Cd *in vivo* changed after binding with FCDs. This may be due to the characteristics of FCDs as nanocarriers, which alter the transport pathways of Cd through features of small size and high specific surface area [44].

Oxidative stress is a crucial toxicological mechanism triggered by NPs or Cd [23,45]. Cd could induce oxidative stress by disrupting the antioxidant system in organisms. When reactive oxygen species (ROS) in contaminated organisms cannot be properly treated by antioxidants, cell stress would be triggered [46]. In our study, as compared to the Cd-treated group, exposure to FCDs-Cd resulted in oxidative stress in zebrafish, manifested by increased mortality, suppressed embryonic hatching rate, and reduced body length. Likewise, FCDs-Cd caused aberrant changes in oxidative stress markers of mice, which was due to the significant accumulation of FCDs-Cd in the liver, kidney, and intestine. Elevated MDA and decreased GSH and SOD indicated oxidative damage and impaired free radical scavenging. This suggested that the antioxidant system was affected by the toxicity of FCDs-Cd and required depletion of antioxidant enzyme activities to maintain homeostasis. Notably, oxidative stress is related to the particle size of NPs, with smaller particles potentially being more capable of penetrating into cells and triggering intracellular oxidative stress responses [47]. FCDs-Cd with small size could more easily penetrate the lipid bilayer and stimulate the production of ROS, thereby provoking inflammatory responses and exacerbating cellular damage.

Biochemical indicators serve as the foundation for the diagnosis of disease and the initial impression for toxicological evaluation. AST and ALT are transaminases in hepatocytes and perform indispensable roles in human metabolism. These enzymes become active when liver cells suffer damage resulting from inflammation, necrosis, or poisoning [48]. In the present study, the AST and ALT levels in the serum were elevated in the mice treated with FCDs-Cd. The aggregation of FCDs-Cd in the kidney resulted in a reduction of glomerular filtration function, which impaired the filtration and excretion of BUN and CR from the bloodstream [49]. MPO is a chemokine secreted in large quantities by activated neutrophils and macrophages during inflammatory responses [50]. NO is a biomarker of inflammation [51]. Here, FCDs-Cd was responsible for promoting elevated NO and MPO in the colon. MPO could promote the production of pro-oxidants and hence cause cross-linking, nitration, oxidation and halogenation reactions of proteins, including antioxidant

enzymes [52]. Meanwhile, NO could react with superoxide radicals to generate peroxynitrite that further increases the ROS content by oxidizing DNA [53]. This suggested that FCDs-Cd ingested through the food chain may accumulate in organs, ultimately contributing to organ damage and dysfunction. In summary, our study demonstrated that FCDs significantly enhanced the toxicity of Cd, forming a synergistic effect by promoting the accumulation of Cd *in vivo* and increasing oxidative stress. However, this study only evaluated the biodistribution and preliminary acute toxicity of FCDs-Cd in vivo, and long-term studies are needed to determine the multi-organ toxicity caused by FCDs-Cd.

Complex pollutants induce oxidative stress and activate transcription factors involved in signaling pathways. In the present study, transcriptome analysis revealed that Syk, PLCy2, Btk, Prkcb, Nfatc1, and Ptpn6 were significantly enriched in B cell receptor signaling pathway, Natural killer cell mediated cytotoxicity, and NF-κB signaling pathway. These genes play a key role in genes related to immune and inflammatory response signals. Syk is a cell membrane non-receptor protein tyrosine kinase that is expressed at high levels in both hematopoietic and non-hematopoietic cells. Upon activation of immune cell receptors, Syk binds to different receptors on the cell surface. Once these receptors engage their ligands, Syk is activated and orchestrates various cellular responses, including cytokine production and phagocytosis [54]. Chemically, Btk is located downstream of Syk, and the activated Syk can phosphorylate Btk [55,56]. PLCγ2 is a signal transducing enzyme that can be activated by tyrosine phosphorylation of receptor kinases and non-receptor kinases. PLCγ2 generates diacylglycerol by hydrolyzing membrane phospholipids, which could activate PKC, so initiating the classical inflammatory pathway cascade of NF-κB [57]. The study showed that PLCγ2 was involved in the downstream signaling pathway of Btk in the mouse aseptic inflammation model, resulting in the activation of Mac-1 and the recruitment of neutrophill [58]. In our study, the expressions of genes such as Btk, PLCγ2 and Prkcb were elevated in the HFCDs-Cd group in comparison to the HCd group, which coincided with the results of H&E staining and NO/MPO activity. This implied that exposure to HFCDs-Cd activated the Syk/Btk/NF-κB pathway, resulting in increased levels of inflammatory factors and subsequently causing injury to the colon tissue of mice. These findings further confirmed the role of FCDs as vectors for Cd, significantly amplifying the toxicity.

5. Conclusions

In summary, this study showed that FCDs could interact with Cd through surface groups to form FCDs-Cd complexes. In contrast, FCDs-Cd exposure led to a significant increase in Cd bioaccumulation in vivo, which exacerbated oxidative stress and produced synergistic effects. These findings reveal the potential biotoxic effects of FCDs interacting with Cd and provide preliminary insights into the bioaccumulation of contaminants in the food chain, which is essential for health risk assessment.

Conflicts of interest

No conflict of interest exists in the submission of this manuscript.

Acknowledgments

This work was supported by the National Key Research and Development Program of China under Grant (2022YFF1102800), the Project of Tianjin Science and Technology Program (22JCYBJC00360) and the Project of Tianjin Science and Technology Program (21ZYJDJC00060). Additional appreciation was extended to the Research Centre of Modern Analytical Technology for the support provided.

References

[1] S. Baraketi, K. Khwaldia, Nanoparticles from agri-food by-products: Green technology synthesis and application in food packaging, Curr. Opin. Green Sustainable Chem. 49 (2024) 100953. https://doi.org/10.1016/j.cogsc.2024.100953

[2] T.A. Saleh, Trends in the sample preparation and analysis of nanomaterials as environmental contaminants, Trends Environ. Anal. Chem. 28 (2020) e00101. https://doi.org/10.1016/j.teac.2020.e00101

[3] J.R. Bi, Y. Li, H.T. Wang, et al., Presence and formation mechanism of foodborne carbonaceous nanostructures from roasted pike eel (*Muraenesox cinereus*), J. Agric. Food. Chem. 66 (2018) 2862-2869. https://doi.org/10.1021/acs.jafc.7b02303

[4] Y.Y. Guo, Y.P. Xiang, G.L. Liu, et al., "Trojan Horse" type internalization increases the bioavailability of mercury sulfide nanoparticles and methylation after intracellular dissolution, ACS Nano 17 (2023) 1925-1934. https://doi.org/10.1021/acsnano.2c05657

[5] C.F. Teng, J.B. Jia, Z.P. Wang, et al., Oral co-exposures to zinc oxide nanoparticles and $CdCl_2$ induced maternal-fetal pollutant transfer and embryotoxicity by damaging placental barriers, Ecotox Environ Safe 189 (2020) 109956. https://doi.org/10.1016/j.ecoenv.2019.1099562024

[6] R.G. Liu, K.J. Liu, M.Q. Tan, Nanocorona formation between foodborne nanoparticles extracted from roast squid and human serum albumin, J. Agric. Food. Chem. (2019) 10470-10480. https://doi.org/10.1021/acs.jafc.9b04425

[7] D.M. Li, X.K. Na, H.T. Wang, et al., Fluorescent carbon dots derived from maillard reaction products: Their properties, biodistribution, cytotoxicity, and antioxidant activity, J. Agric. Food. Chem. 66 (2018) 1569-1575. https://doi.org/10.1021/acs.jafc.7b05643

[8] Y.Y. Liu, N.Y. Yu, W.D. Fang, et al., Photodegradation of carbon dots cause cytotoxicity, Nat. Commun. 12 (2021) 812. https://doi.org/10.1038/s41467-021-21080-z

[9] N. Oladzadabbasabadi, M.A. Dheyab, A.M. Nafchi, et al., Turning food waste into value-added carbon dots for sustainable food packaging application: A review, Adv. Colloid Interface Sci. 321 (2023) 103020. https://doi.org/10.1016/j.cis.2023.103020

[10] H.Z. Fan, M. Zhang, B. Bhandari, et al., Food waste as a carbon source in carbon quantum dots technology and their applications in food safety detection, Trends Food Sci Tech 95 (2020) 86-96. https://doi.org/10.1016/j.tifs.2019.11.008

[11] M. Moradi, R. Molaei, S.A. Kousheh, et al., Carbon dots synthesized from microorganisms and food by-products: Active and smart food packaging applications, Crit. Rev. Food Sci. Nutr. 63(2023) 1943-1959. https://doi.org/10.1080/10408398.2021.2015283

[12] Y.K. Song, Y.Y. Wu, H.T. Wang, et al., Carbon quantum dots from roasted Atlantic salmon (*Salmo salar* L.): Formation, biodistribution and cytotoxicity, Food Chem. 293 (2019) 387-395. https://doi.org/10.1016/j.foodchem.2019.05.017

[13] B.Y. Zhang, X.P. Fan, H.N. Du, et al., Foodborne carbon dot exposure induces insulin resistance through gut microbiota dysbiosis and damaged intestinal mucus layer, ACS Nano 17 (2023) 6081-6094. https://doi.org/10.1021/acsnano.3c01005

[14] K.J. Liu, Y.K. Song, M.Q. Tan, Toxicity alleviation of carbon dots from roast beef after the formation of protein coronas with human serum albumin, J. Agric. Food. Chem. 68 (2020) 9789-9795. https://doi.org/10.1021/acs.jafc.0c03499

[15] J.X. Geng, X.Y. Song, X.D. Zhang, et al., Hydrophilic food-borne nanoparticles from beef broth as novel nanocarriers for zinc, J. Agric. Food. Chem. 67 (2019) 6995-7004. https://doi.org/10.1021/acs.jafc.9b01372

[16] N.Y. Wang, Y.Y. Wu, X. Zhao, et al., Food-borne nanocarriers from roast beef patties for iron delivery, Food Funct. 10 (2019) 6711-6719. https://doi.org/10.1039/c9fo01795j

[17] S.V. Koparde, O.S. Nille, A.G. Kolekar, et al., Okra peel-derived nitrogen-doped carbon dots: Eco-friendly synthesis and multi-functional applications in heavy metal ion sensing, nitro compound detection and environmental remediation, Spectrochim Acta A 321 (2024) 124659. https://doi.org/10.1016/j.saa.2024.124659

[18] Y. Huang, F. Feng, Z.G. Chen, et al., Green and efficient removal of cadmium from rice flour using natural deep eutectic solvents, Food Chem. 244 (2018) 260-265. https://doi.org/10.1016/j.foodchem.2017.10.060

[19] A. Åkesson, L. Barregard, I.A. Bergdahl, et al., Non-renal effects and the risk assessment of environmental cadmium exposure, Environ. Health Perspect. 122 (2014) 431-438. https://doi.org/10.1289/ehp.1307110

[20] Y.Y. Yu, B.B. Tong, Y. Liu, et al., Bioaccumulation, histopathological and apoptotic effects of waterborne cadmium in the intestine of crucian carp *Carassius auratus gibelio*, Aquacult. Rep. 20 (2021) 100669. https://doi.org/10.1016/j.aqrep.2021.100669

[21] Y.H. Wang, W.J. Gu, Z.L. Xu, et al., Comprehensive multi-omics investigation of sub-chronic toxicity induced by cadmium and triazophos co-exposure in hook snout carps (*Opsariichthys bidens*), J. Hazard. Mater. 476 (2024) 135104. https://doi.org/10.1016/j.jhazmat.2024.135104

[22] M. Waisberg, P. Joseph, B. Hale, et al., Molecular and cellular mechanisms of cadmium carcinogenesis, Toxicology 192 (2003) 95-117. https://doi.org/10.1016/s0300-483x(03)00305-6

[23] M.C Guo, X.L. Xu, X.C. Yan, et al., *In vivo* biodistribution and synergistic toxicity of silica nanoparticles and cadmium chloride in mice, J. Hazard. Mater. 260 (2013) 780-788. https://doi.org/10.1016/j.jhazmat.2013.06.040

[24] X.Y. Song, L. Cao, S. Cong, et al., Characterization of endogenous nanoparticles from roasted chicken breasts, J. Agric. Food. Chem. 66 (2018) 7522-7530. https://doi.org/10.1021/acs.jafc.8b01988

[25] T. Zhang, Z.C. Xu, L. Wen, et al., Cadmium-induced dysfunction of the blood-brain barrier depends on ROS-mediated inhibition of PTPase activity in zebrafish, J. Hazard. Mater. 412 (2021) 125198. https://doi.org/10.1016/j.jhazmat.2021.125198

[26] Z.H. Zhao, J.S. Hyun, H. Satsu, et al., Oral exposure to cadmium chloride triggers an acute inflammatory response in the intestines of mice, initiated by the over-expression of tissue macrophage inflammatory protein-2 mRNA, Toxicol. Lett. 164 (2006) 144-154. https://doi.org/10.1016/j.toxlet.2005.12.004

[27] X.N. Tian, G.L. Wang, K.N. Jin, et al., Rice hull insoluble dietary fiber alleviated experimental colitis induced by low dose of dextran sulfate sodium in cadmium-exposed mice, Food Funct. 13 (2022) 7215-7225. https://doi.org/10.1039/d2fo00891b

[28] Y. Zhou, W. Chen, S. Feng, et al., Ochratoxin A-induced mitochondrial pathway apoptosis and ferroptosis by promoting glycolysis, Apoptosis. 30 (2025) 1440-1452. https://doi.org/10.1007/s10495-025-02109-w.

[29] J. Wang, X.L. Zheng, H.F. Zhang, Exploring the conformational changes in fibrinogen by forming protein corona with CdTe quantum dots and the related cytotoxicity, Spectrochim Acta A 220 (2019) 117143. https://doi.org/10.1016/j.saa.2019.117143

[30] L.M. Browning, T. Huang, X.H. Xu, Real-time *in vivo* imaging of size-dependent transport and toxicity of gold nanoparticles in zebrafish embryos using single nanoparticle plasmonic spectroscopy, Interface Focus 3 (2013) 20120098. https://doi.org/10.1098/rsfs.2012.0098

[31] W.Y. Qiu, J.L. Ye, Y.M. Su, et al., Co-exposure to environmentally relevant concentrations of cadmium and polystyrene nanoplastics induced oxidative stress, ferroptosis and excessive mitophagy in mice kidney, Environ. Pollut. 333 (2023) 121947. https://doi.org/10.1016/j.envpol.2023.121947

[32] H. Feng, Y. Liu, Y. Xu, et al., Benzo[a]pyrene and heavy metal ion adsorption on nanoplastics regulated by humic acid: Cooperation/competition mechanisms revealed by molecular dynamics simulations, J. Hazard. Mater. 424 (2022) 127431. https://doi.org/10.1016/j.jhazmat.2021.127431

[33] B.Y. Zhang, L.D. Yu, R.J. Zhu, et al., Malting barley carbon dots-mediated oxidative stress promotes insulin resistance in mice via NF-κB pathway and MAPK cascade, J. Nanobiotechnol. 20 (2022) 331. https://doi.org/10.1186/s12951-022-01543-1

[34] M.M. Jia, B.C. Yi, X. Chen, et al., Carbon dots induce pathological damage to the intestine via causing intestinal flora dysbiosis and intestinal inflammation, J. Nanobiotechnol. 21 (2023) 167. https://doi.org/10.1186/s12951-023-01931-1

[35] X.M. Chen, M.Y. Bi, J. Yang, et al., Cadmium exposure triggers oxidative stress, necroptosis, Th1/Th2 imbalance and promotes inflammation through the TNF-α/NF-κB pathway in swine small intestine, J. Hazard. Mater. 421 (2022) 126704. https://doi.org/10.1016/j.jhazmat.2021.126704

[36] B. van Dam, H. Nie, B. Ju, et al., Excitation-dependent photoluminescence from single-carbon dots, Small 13 (2017) 1702098. https://doi.org/10.1002/smll.201702098

[37] J. Fu, L. Wang, H.Q. Chen, et al., A selective fluorescence probe for mercury ion based on the fluorescence quenching of terbium (III)-doped cadmium sulfide composite nanoparticles, Spectrochim Acta A 77 (2010) 625-629.

https://doi.org/10.1016/j.saa.2010.06.038

[38] Y.R. Li, K. Wang, S. Dötterl, et al., The critical role of organic matter for cadmium-lead interactions in soil: Mechanisms and risks, J. Hazard. Mater. 476 (2024) 135123. https://doi.org/10.1016/j.jhazmat.2024.135123

[39] H.T. Wang, S. Liu, Y.K. Song, et al., Universal existence of fluorescent carbon dots in beer and assessment of their potential toxicity, Nanotoxicology 13 (2019) 160-173. https://doi.org/10.1080/17435390.2018.1530394

[40] C. Jadán-Piedra, G.M. Chiocchetti, M.J. Clemente, et al., Dietary compounds as modulators of metals and metalloids toxicity, Crit. Rev. Food Sci. Nutr. 58 (2018) 2055-2067. https://doi.org/10.1080/10408398.2017.1302407

[41] S.Chen, H.G. Gan, X.Y. Lin, et al., Microplastic co-exposure elevates cadmium accumulation in mouse tissue after rice consumption: Mechanisms and health implications, J. Hazard. Mater. 476 (2024) 135218. https://doi.org/10.1016/j.jhazmat.2024.135218

[42] L.H. Hu, X.Y. Feng, Y.Z. Lan, et al., Co-exposure with cadmium elevates the toxicity of microplastics: Trojan horse effect from the perspective of intestinal barrier, J. Hazard. Mater. 466 (2024) 133587. https://doi.org/10.1016/j.jhazmat.2024.133587

[43] Z. Kayaaltı, D.K. Akyüzlü, T. Söylemezoğlu, Evaluation of the effect of divalent metal transporter 1 gene polymorphism on blood iron, lead and cadmium levels, Environ. Res. 137 (2015) 8-13. https://doi.org/10.1016/j.envres.2014.11.008

[44] P. Liu, S. Wang, Z.M. Chang, et al., Combined toxicity of silica nanoparticles and cadmium chloride on the cardiovascular system of zebrafish (*Danio rerio*) larvae, Comp Biochem Phys C 239 (2021) 108895. https://doi.org/10.1016/j.cbpc.2020.108895

[45] K. Khosravi-Katuli, A. Shabani, H. Paknejad, et al., Comparative toxicity of silver nanoparticle and ionic silver in juvenile common carp (*Cyprinus carpio*): Accumulation, physiology and histopathology, J. Hazard. Mater. 359 (2018) 373-381. https://doi.org/10.1016/j.jhazmat.2018.07.064

[46] Y.Y. Wu, W.F. Tian, C.X. Cheng, et al., Effects of cadmium exposure on metabolism, antioxidant defense, immune function, and the hepatopancreas transcriptome of *Cipangopaludina cathayensis,* Ecotox Environ Safe 264 (2023), 115416. https://doi.org/10.1016/j.ecoenv.2023.115416

[47] X. Du, M.L. Zhang, Y.R. Ma, et al., Size-dependent antibacterial of carbon dots by selective absorption and differential oxidative stress of bacteria, J. Colloid Interface Sci. 634 (2023) 44-53. https://doi.org/10.1016/j.jcis.2022.12.025

[48] X.N. Tian, Y.X. Ding, Y. Kong, et al., Purslane (*Portulacae oleracea* L.) attenuates cadmium-induced hepatorenal and colonic damage in mice: Role of chelation, antioxidant and intestinal microecological regulation, Phytomedicine 92 (2021) 153716. https://doi.org/10.1016/j.phymed.2021.153716

[49] G. Pallio, A. Micali, S. Benvenga, et al., Myo-inositol in the protection from cadmium-induced toxicity in mice kidney: An emerging nutraceutical challenge, Food Chem. Toxicol. 132 (2019) 110675. https://doi.org/10.1016/j.fct.2019.110675

[50] G. Ndrepepa, Myeloperoxidase-A bridge linking inflammation and oxidative stress with cardiovascular disease, Clin. Chim. Acta 493 (2019) 36-51. https://doi.org/10.1016/j.cca.2019.02.022

[51] M. Zhang, C.L. Tong, Real-time and specific monitoring of nitric oxide and evaluating of the oxidative stress in living cells and zebrafish under the pollutant exposure using a carbon dot-based composite fluorescent probe, J. Hazard. Mater. 472 (2024) 134558. https://doi.org/10.1016/j.jhazmat.2024.134558

[52] R.L. Zhang, M.L. Brennan, Z.Z. Shen, et al., Myeloperoxidase functions as a major enzymatic catalyst for initiation of lipid peroxidation at sites of inflammation, J Biol. Chem. 277 (2002) 46116-46122. https://doi.org/10.1074/jbc.M209124200

[53] P. Pacher, J.S. Beckman, L. Liaudet, Nitric oxide and peroxynitrite in health and disease, Physiol. Rev. 87 (2007) 315-424. https://doi.org/10.1152/physrev.00029.2006

[54] M. Knoll, S. Winther, A. Natarajan, et al., SYK kinase mediates brown fat differentiation and activation, Nat. Commun. 8 (2017) 2115. https://doi.org/10.1038/s41467-017-02162-3

[55] H. Mueller, A. Stadtmann, H. Van Aken, et al., Tyrosine kinase Btk regulates E-selectin-mediated integrin activation and neutrophil recruitment by controlling phospholipase C (PLC) gamma2 and PI3Kgamma pathways, Blood 115 (2010) 3118-27. https://doi.org/10.1182/blood-2009-11-254185

[56] X.Z. Zhang, D. Mei, H. Wang, et al., hIgDFc-Ig inhibits B cell function by regulating the BCR-Syk-Btk-NF-κB signalling pathway in mice with collagen-induced arthritis, Pharmacol. Res. 173 (2021) 105873. https://doi.org/10.1016/j.phrs.2021.105873

[57] J. Obst, H.L. Hall-Roberts, T.B. Smith, et al., PLCγ2 regulates TREM2 signalling and integrin-mediated adhesion and migration of human iPSC-derived macrophage, Sci. Rep. 11 (2021) 19842. https://doi.org/10.1038/s41598-021-96144-7

[58] S. Volmering, H. Block, M. Boras, et al., The neutrophil Btk signalosome regulates integrin activation during sterile inflammation, Immunity 44 (2016) 73-87. https://doi.org/10.1016/j.immuni.2015.11.011